



HAL
open science

Propagation of electromagnetic waves through the Martian ionosphere

Olga Melnik, Michel Parrot

► **To cite this version:**

Olga Melnik, Michel Parrot. Propagation of electromagnetic waves through the Martian ionosphere. *Journal of Geophysical Research Space Physics*, 1999, 104 (A6), pp.12705-12714. 10.1029/1999JA900100 . insu-03234946

HAL Id: insu-03234946

<https://insu.hal.science/insu-03234946>

Submitted on 25 May 2021

HAL is a multi-disciplinary open access archive for the deposit and dissemination of scientific research documents, whether they are published or not. The documents may come from teaching and research institutions in France or abroad, or from public or private research centers.

L'archive ouverte pluridisciplinaire **HAL**, est destinée au dépôt et à la diffusion de documents scientifiques de niveau recherche, publiés ou non, émanant des établissements d'enseignement et de recherche français ou étrangers, des laboratoires publics ou privés.

Propagation of electromagnetic waves through the Martian ionosphere

Olga Melnik and Michel Parrot

Laboratoire de Physique et Chimie de l'Environnement, Centre National de la Recherche Scientifique Orléans, France

Abstract. This paper is related to the study of ELF-VLF wave propagation through the Martian ionosphere using a WKB method. It is expected that waves coming from the atmosphere could be observed by a probe in orbit around Mars. Characteristics of the wave propagation have been determined from Maxwell's equations. The ionospheric conductivities have been calculated using known parameters of the Martian ionosphere in different cases: nightside and dayside, low and high solar activity, and low and high magnetic field. It is shown that ELF-VLF waves with a maximum frequency ~ 4000 Hz can only propagate if we consider a strong magnetic field on the nightside and a low solar activity.

1. Introduction

The Martian atmosphere is too tenuous to have lightning as on the Earth. But electrical discharge may occur in the large dust and sand storms which exist on this planet. In a previous paper, *Melnik and Parrot* [1998] showed with a numerical simulation that such events are possible. When it occurs, this electrical discharge is able to generate electromagnetic waves in a broad frequency range. As waves can propagate in the atmosphere and then in the ionosphere, it could be possible to observe these emissions with a probe in a low orbit around Mars. However, attenuation or even complete reflection of the waves could occur in the ionosphere depending on the wave frequencies and on plasma parameters. The purpose of this paper is to check the propagation characteristics of these electromagnetic waves through the Martian ionosphere using a WKB method. The approach to investigate the problem is similar to the work of *Huba and Rowland* [1993] who studied the wave propagation through the ionosphere of Venus.

The analytical expression of the wave dispersion relation is calculated in section 2. Section 3 presents the variations of the ionospheric parameters which have been obtained from a search of the literature in order to numerically evaluate the dispersion relation. Simplified solutions for specific frequency ranges are given in section 4, whereas the main results are shown in section 5. Finally, conclusions are given in section 6.

2. Dispersion Relation

The equations for the electric field \mathbf{E} and for the magnetic field \mathbf{B} are derived from the Maxwell equations:

$$\begin{aligned} \frac{\partial \mathbf{B}}{\partial t} &= -\nabla \times \mathbf{E} \\ \frac{1}{c^2} \frac{\partial \mathbf{E}}{\partial t} &= \nabla \times \mathbf{B} - \mu_0 \mathbf{j} = \nabla \times \mathbf{B} - \mu_0 \sigma \cdot \mathbf{E} \end{aligned} \quad (1)$$

where the first equation is Faraday's law and the second is Ampere's law; c is the velocity of light, μ_0 is the permeability of free space, and σ is the conductivity tensor (see appendix A). We will consider an orthogonal Cartesian coordinate system (x, y, z) where the z axis is vertical. The Martian magnetic field \mathbf{B}_0 is directed toward the z direction, and we will study the propagation of waves parallel to \mathbf{B}_0 , i.e., with a wave normal along the z axis. Then the transverse field can be written as

$$\begin{aligned} \mathbf{E} &= E_x \mathbf{x} + E_y \mathbf{y} \\ \mathbf{B} &= B_x \mathbf{x} + B_y \mathbf{y} \end{aligned} \quad (2)$$

The temporal and spatial variations of the components $E_x, E_y, B_x,$ and B_y are $\propto \exp i(\omega t - kz)$, where ω is the angular frequency and k is the wave number. Relative to the electric components and using the components of the conductivity tensor (see appendix A, equation (A2)), equation (1) can be written as

$$\begin{aligned} \left(\frac{\omega^2}{c^2} - k^2 - i\omega\mu_0\sigma_p\right)E_x - i\omega\mu_0\sigma_H E_y &= 0 \\ \left(\frac{\omega^2}{c^2} - k^2 - i\omega\mu_0\sigma_p\right)E_y + i\omega\mu_0\sigma_H E_x &= 0 \end{aligned} \quad (3)$$

Using the complex function $F_{\pm} = E_x \pm iE_y$, equation (3) can be written in the simplified form:

$$\left[\frac{\omega^2}{c^2} - k^2 - \omega\mu_0(i\sigma_p \pm \sigma_H)\right]F_{\pm} = 0 \quad (4)$$

With $\epsilon_0\mu_0c^2 = 1$, the dispersion relation becomes

$$k^2 = \frac{\omega^2}{c^2} \left[1 - \frac{1}{\omega\epsilon_0} (i\sigma_p \pm \sigma_H)\right] \quad (5)$$

We will only study the case of the right mode waves F_+ which will be written F in the following sections. In a two-component plasma, the conductivities σ_p and σ_H depend on the collision frequencies, the plasma frequency, the electron gyrofrequency, and the ion gyrofrequency. Their analytical expressions are given in appendix A. The quantities needed to evaluate the conductivities are given in section 3.

3. Martian Ionospheric Parameters

The wave propagation has been studied during low and high solar activity and for the dayside and nightside of the ionosphere. The relevant ionospheric parameters are obtained from experimental results (Mariner, Viking) or from models. Neutral densities are given by *Winchester and Rees* [1995] and *Fox et al.* [1996]. The densities are measured during low solar activity and on the dayside. In the absence of other measurements, we used these values for all cases. The total neutral density in the altitude range we survey is given in Figure 1. Densities of major ions on the dayside and during a low solar activity have been presented by *Shinagawa and Cravens* [1989], *Winchester and Rees* [1995], and *Fox et al.* [1996]. The same parameters during a high solar activity have been obtained by *Fox et al.* [1996]. Densities of major ions on the nightside and during low and high solar activity are given by *Haider* [1997] and *Fox et al.* [1993], respectively. In the following, we will assume that we have equilibrium, i.e., the sum of the ion densities is equal to the electron density in all cases. Figure 2 represents the total ion density as a function of altitude. In Figure 2a, the solid line and the dashed line are related to a low and high solar activity, respectively, on the dayside, whereas the same curves in Figure 2b are related to data on the nightside. The values are in agreement with the electron densities provided by *Fox et al.* [1996] for low and high solar activity on the dayside and by *Haider* [1997] for a low solar activity on the nightside. The electron temperature data, which are adapted from *Fox et al.* [1996], are represented in Figure 3.

Therefore, using data of Figures 1-3, the collision frequencies given by (A7) can be evaluated for the different conditions. They are represented in Figure 4.

Two models of the Martian magnetic field have been used. They are plotted in Figure 5. Figure 5a shows an adaption of the induced magnetic field calculated by *Shinagawa and Cravens* [1989], whereas Figure 5b shows a field variation extrapolated from the recent measurement from Mars Global Surveyor by *Acuña et al.* [1998]. They have shown that the intrinsic Martian magnetic field

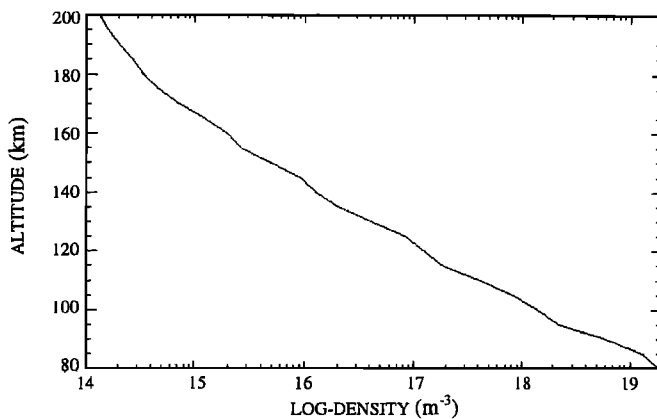


Figure 1. Total neutral density as a function of altitude.

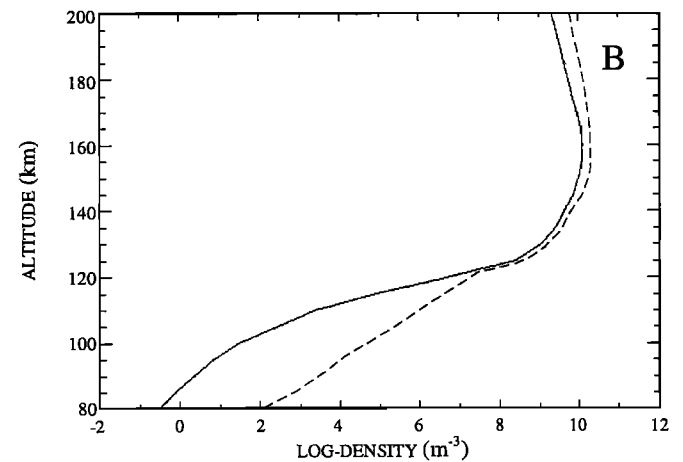
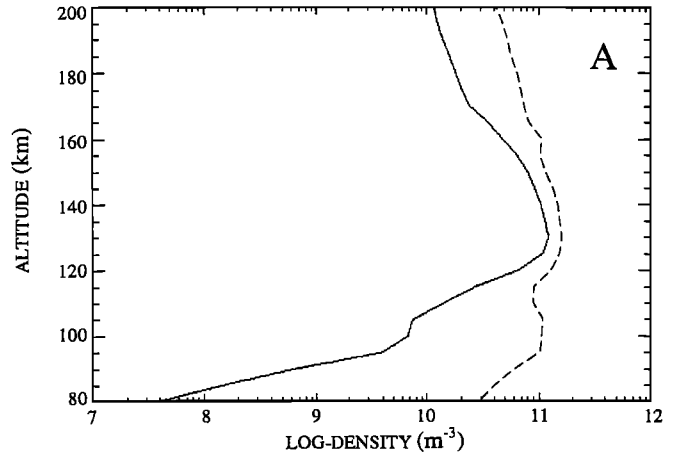


Figure 2. Total ion density as a function of altitude. The solid line and the dashed line are related to a low and high solar activity, respectively, on (a) the dayside and (b) the nightside.

could be as high as 400 nT at some locations. As examples, the gyrofrequency of the ion O^+ which is considered as the main ion in this study, the electron gyro-frequency, and the plasma frequency $\omega_{pe} = (n_e e^2 / \epsilon_0 m_e)^{1/2}$ (see appendix A) are plotted in Figure 6 for the nightside and during low solar activity. Figure 6a is related to the magnetic field shown in Figure 5a, whereas Figure 6b is related to the field shown in Figure 5b.

4. Approximate Solutions

Figures 4 and 5 define eight different cases, and, in a first time, rough solutions can be evaluated to determine if propagation is possible.

4.1. Low Solar Activity and on the Nightside

Approximate values of the conductivities (A6) are calculated for a low solar activity, and on the nightside, in order to obtain rough solutions of the wave equation (4) in given frequency ranges.

4.1.1. Induced magnetic field. This case corresponds to Figures 4a and 6a. At the lower edge, it is observed that $v_{en} \gg v_{ci}, v_{ie}$, that v_{en}

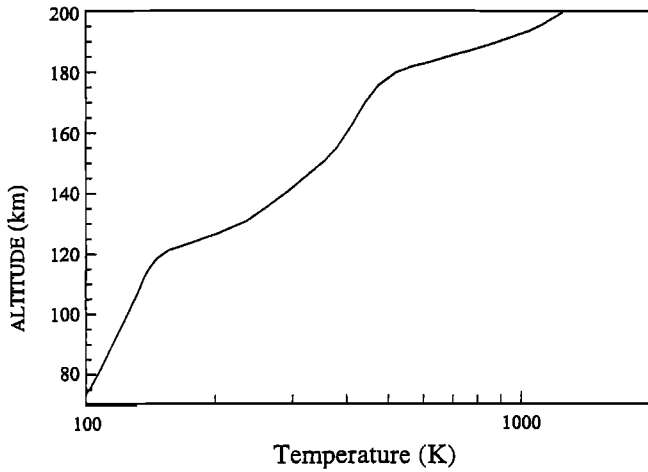


Figure 3. Electron temperature as a function of altitude.

$\gg |\Omega_e|$, and that $|\Omega_e| \gg \Omega_i$. Then, the equations (A6) can be written

$$\begin{aligned} \sigma_p &= \frac{n_e e^2}{m_e} \frac{1}{(v_{en} + i\omega)} \\ \sigma_H &= \frac{n_e e^2}{m_e} \frac{\Omega_e}{(v_{en} + i\omega)^2} \end{aligned} \quad (6)$$

From (5) and noticing that $\sigma_p \gg |\sigma_H|$, a simplified dispersion relation at the lower edge is

$$k^2 = \frac{\omega^2}{c^2} \left[1 - i \frac{\omega_{pe}^2}{\omega (v_{en} + i\omega)} \right] \quad (7)$$

The condition $\omega \ll v_{en}$ in equation (7) gives

$$N^2 = 1 - i \frac{\omega_{pe}^2}{\omega v_{en}} \quad (8)$$

where N is the refractive index (kc/ω). Equation (8) shows that waves are attenuated when they propagate from the lower ionosphere up to altitudes where the ionization and the magnetic field play essential roles. In the opposite case, $\omega \gg v_{en}$, we have

$$N^2 = 1 - \frac{\omega_{pe}^2}{\omega^2} \quad (9)$$

and the waves are propagating without attenuation.

At higher altitudes (> 120 km), the plasma frequency is larger and we can expect a large attenuation of waves propagating in the whistler mode. The collision frequencies are roughly of the same order ($v_{en} \sim v_{in} \sim v_{ei}$) and $|\Omega_e| \gg v_{a\beta}$.

With the condition $\omega \gg v_{a\beta}$, the conductivities become

$$\begin{aligned} \sigma_p &= i \frac{n_e e^2}{m_e} \frac{\omega}{\Omega_e^2 - \omega^2} \\ \sigma_H &= \frac{n_e e^2}{m_e} \frac{\Omega_e}{\Omega_e^2 - \omega^2} \end{aligned} \quad (10)$$

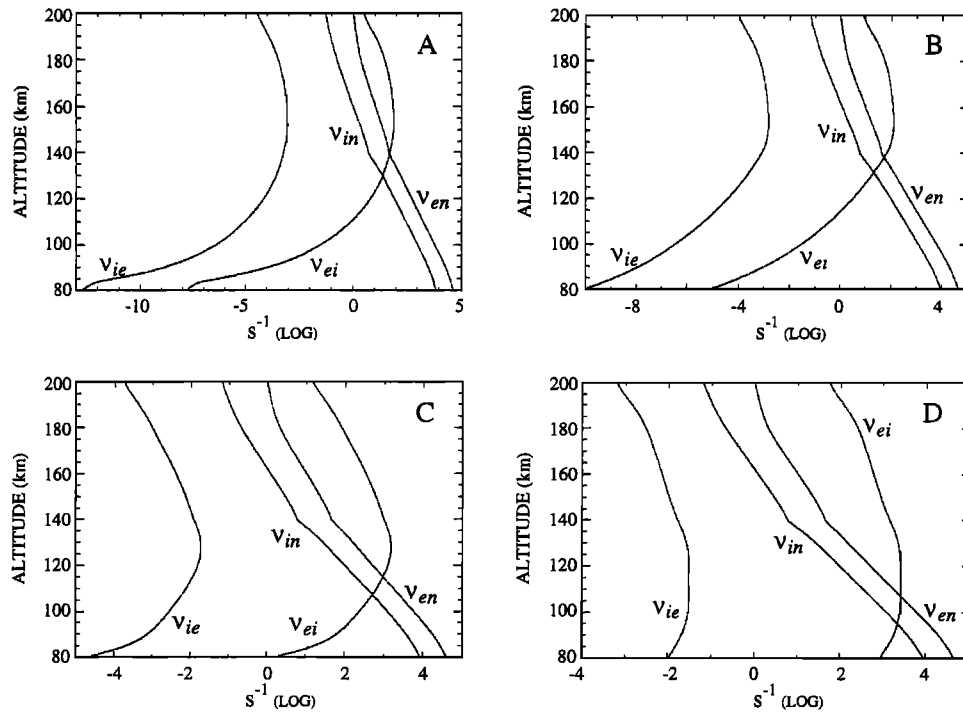


Figure 4. Collision frequencies $v_{a\beta}$ as a function of altitude (i ion; e electron; n neutral) during (a) low solar activity on the nightside, (b) high solar activity on the nightside, (c) low solar activity on the dayside, (d) high solar activity on the dayside.

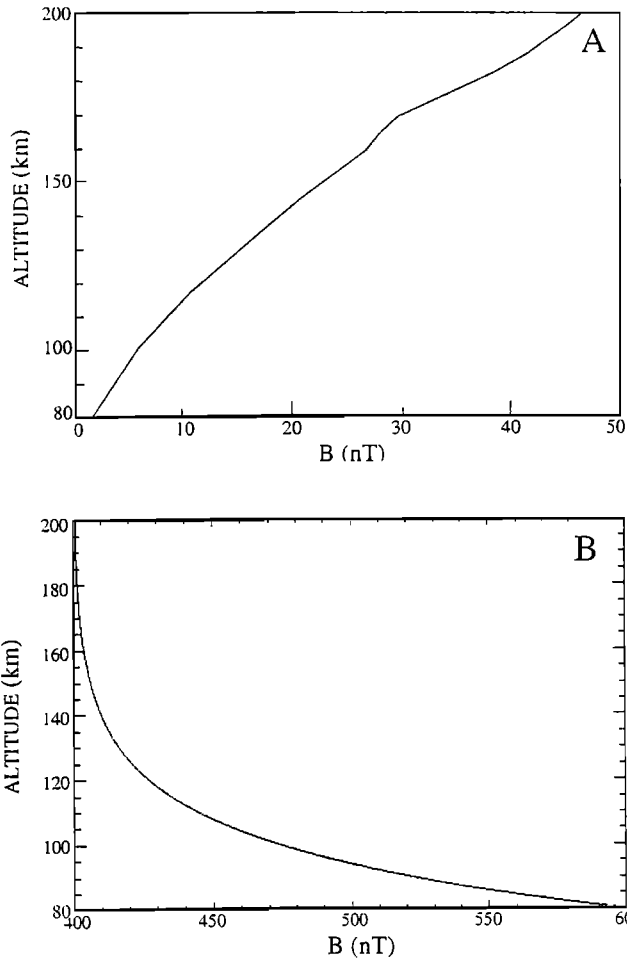


Figure 5. Magnetic field as a function of altitude. (a) Induced magnetic field adapted from *Shinagawa and Cravens* [1989] and (b) intrinsic magnetic field (see text).

The Pedersen conductivity is purely imaginary and the Hall conductivity is purely real. The refractive index is

$$N^2 = 1 - \frac{\omega_{pe}^2}{\omega(\omega + \Omega_e)} \quad (11)$$

The waves can propagate in the frequency band $v_{ap} \ll \omega < |\Omega_e|$ as it is expected. For high frequency ($\omega \gg |\Omega_e|$), the refractive index, which is given by (9), indicates that the propagation is possible for waves with $\omega > \omega_{pe}$ as usual. When the frequencies are lower and similar to the collision frequencies $v_{en,ei}$ the propagation is impossible. In this case (induced magnetic field, low solar activity, and nightside), there is no propagation because the refractive index at the lower edge of the ionosphere is given by (8).

4.1.2. Intrinsic magnetic field. This case corresponds to Figures 4a and 6b. At the lower edge, we have the conditions $v_{en} \gg v_{ei,te}$ and $|\Omega_e| > v_{en}$; the conductivities are

$$\begin{aligned} \sigma_p &= \frac{n_e e^2}{m_e} \frac{v_{en} + i\omega}{\Omega_e^2 + (v_{en} + i\omega)^2} \\ \sigma_H &= \frac{n_e e^2}{m_e} \frac{\Omega_e}{\Omega_e^2 + (v_{en} + i\omega)^2} \end{aligned} \quad (12)$$

and then, if $\omega \ll v_{en}$, the refractive index is

$$N^2 = 1 - \frac{\omega_{pe}^2}{\omega(\Omega_e - iv_{en})} \quad (13)$$

which means that the waves can propagate with little attenuation in the layers where the approximation is valid. When the frequencies are equal to the collision frequencies between neutral and charged particles, the attenuation is preponderant.

For the ionospheric layers between ~120 km and ~170 km, the refractive index is given by equation (11). The waves with frequencies $\omega \gg v_{ap}$ are propagating with little attenuation. The waves with lower frequencies ($\omega \sim v_{ap}$) are more attenuated.

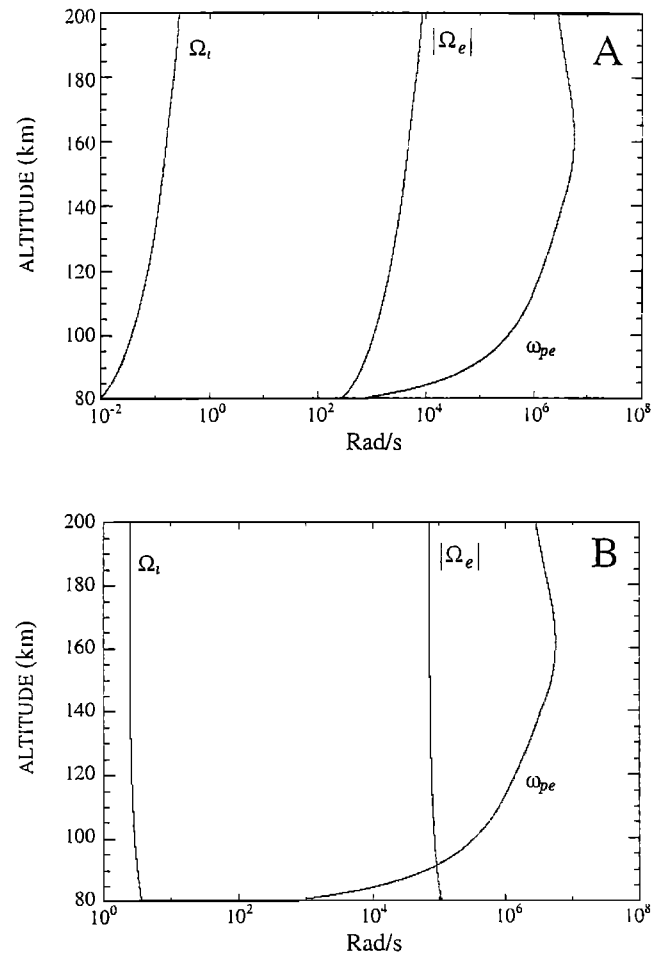


Figure 6. Representation of the O^+ gyrofrequency Ω_o , the electron gyrofrequency $|\Omega_e|$, and the plasma frequency ω_{pe} as function of altitude in case of (a) an induced low magnetic field and (b) an intrinsic magnetic field (see text).

In the upper ionosphere, the collision frequencies decrease, and equation (11) is valid in the frequency range $\nu_{cp} \ll \omega < |\Omega_e|$. The waves with frequencies in this range propagate with very little attenuation. In this case (intrinsic magnetic field, low solar activity, and nightside), the conditions of propagation are favorable through all ionospheric layers.

4.2. Other Cases

Figure 4b, which concerns the case "high solar activity and on the nightside", is very similar to Figure 4a, and therefore the conditions for propagation described in sections 4.1.1 and 4.1.2 are valid. Propagation is only possible when the magnetic field is strong enough.

On the dayside, ionization is much more important than on the nightside and the collision frequencies between charged particles increase as it is seen in Figures 4c (low solar activity) and 4d (high solar activity). Therefore the same case as in section 4.1.1 but on the dayside corresponds to a worse situation because $\nu_{en} \sim |\Omega_e|$ between 90 and 140 km. For a strong magnetic field, the propagation during low solar activity is also not possible because the condition $\nu_{en} \gg \nu_{en}$ used in section 4.1.1, is only valid at the lower edge of the ionosphere. The conditions of propagation relative to the case "high solar activity and on the dayside" (Figure 4d) are much more unfavorable than during low solar activity whatever is the intensity of the magnetic field.

5. Results

For HF waves with frequency larger than the plasma frequency, there is no propagation problem. However, considering the approximations of the solutions in different cases which are detailed in section 4, it is clear that the ELF-VLF wave propagation will only occur on the nightside and when the magnetic field is strong enough. The solution of equation (4) is given in appendix B. We studied waves in a frequency range from 10 Hz to 10 kHz. The results for the nightside case with a strong magnetic field and a low solar activity are shown in Figure 7. The imaginary part and the real part of the square of the wave number amplitude are shown for different frequencies in Figures 7a and 7b, respectively. A condition to have small wave attenuation is that the real part of the amplitude of the wave number k is much larger than the imaginary part. Figure 7c represents the wave amplitude for different frequencies. The dashed, dotted, and solid lines represent the real part, the imaginary part, and the modulus of F as function of altitude, respectively. To plot the curves, we have chosen at 80 km an arbitrary value of the wave modulus A equal to 1 mV/m in the system of equations (B9). At $f = 10$ Hz, it is shown that the wave propagates without attenuation up to 120 km but that it suffers moderate attenuation above 120 km. At higher frequencies (from ~ 100 Hz up to ~ 5 kHz), the wave amplitude is also reduced but can reach the topside ionosphere. When the frequency is larger than 6 kHz, the waves are entirely attenuated in the first ionospheric layers. Figure 8 is similar to Figure 7, but it concerns the case of high solar activity. It can be observed that the features are more or less identical with the following differences: (1) The maximum frequency of waves reaching the topside ionosphere is smaller and (2) for a given frequency, the amplitude of the waves at 200 km is smaller than in the previous case. These two points are detailed in Figure 9, which shows the percentage of the wave amplitude for waves reaching the topside ionosphere as a function of frequency. Figure 9a is related

to Figure 7 (low solar activity), whereas Figure 9b is related to Figure 8 (high solar activity). In the two cases, the percentage decreases slowly with the frequency but with a slope which is slightly different (at 1 kHz for example, the attenuation is $\sim 56\%$ for the low solar activity, whereas it is $\sim 38\%$ for the high solar activity). It is confirmed that the maximum frequency of propagating waves is larger for low solar activity (~ 4000 Hz).

The validity of the WKB approximation is discussed in appendix B, and application of equation (B10) to the above cases indicates that problems could appear for frequencies < 100 Hz between 80 and 100 km. It is the lower edge of our analysis domain, and then the WKB method used to study the wave propagation has no implication on the results.

6. Conclusions

The propagation of ELF-VLF electromagnetic waves through the Martian ionosphere has been investigated. This work used the ionospheric parameters which have been measured during past experiments or obtained with models. It shows that if we consider a low magnetic field induced by the solar wind, no propagation of waves from the atmosphere up to the top ionosphere would be possible. The waves will only propagate through the ionosphere if the Martian magnetic field is strong enough. The probe Mars Global Surveyor has shown that such high value could occur above specific regions of the Martian surface. In such a case we have shown that the waves can propagate on the nightside. The frequency window is larger and the amplitude attenuation is lower during low solar activity than during high solar activity. Waves with frequencies less than 4 kHz are able to go through the ionosphere during low solar activity. Their attenuation is frequency dependent. We assume in our calculations that the ionosphere is uniform. In the case of ionospheric irregularities, propagation is always possible in guides.

For simplicity, the special case of propagation along the magnetic field has been considered. It is expected that oblique waves will be more strongly attenuated because of their longer ray paths in the collisional ionospheric layers.

This work was undertaken as part of the wave experiment ELISMA on board the MARS 96 mission [ELISMA Experimenters, 1998]. The main scientific objective of ELISMA was to study the electromagnetic waves in the Martian ionosphere, but, unfortunately, the launch of MARS 96 failed. Another wave experiment has been recently launched onboard the Japanese mission PLANET-B [Tsuruda *et al.*, 1996].

Another application of this study is related to the possibility of using HF radio on Mars. In the future, communications between several bases on the surface of Mars may be needed without the help of an orbiter [Fry and Yowell, 1994], and working frequency for these must be chosen. Waves with frequencies larger than the plasma frequency will not be reflected by the ionosphere. The maximum values of the plasma frequency are ~ 0.9 , 1.2, 2.7, and 3.7 MHz for the nightside during low solar activity, the nightside during high solar activity, the dayside during low solar activity, and the dayside during high solar activity, respectively.

Appendix A: Conductivity Tensor

Ohm's law with an electric field \mathbf{E} can be written as

$$\mathbf{j} = \sigma \cdot \mathbf{E} \quad (\text{A1})$$

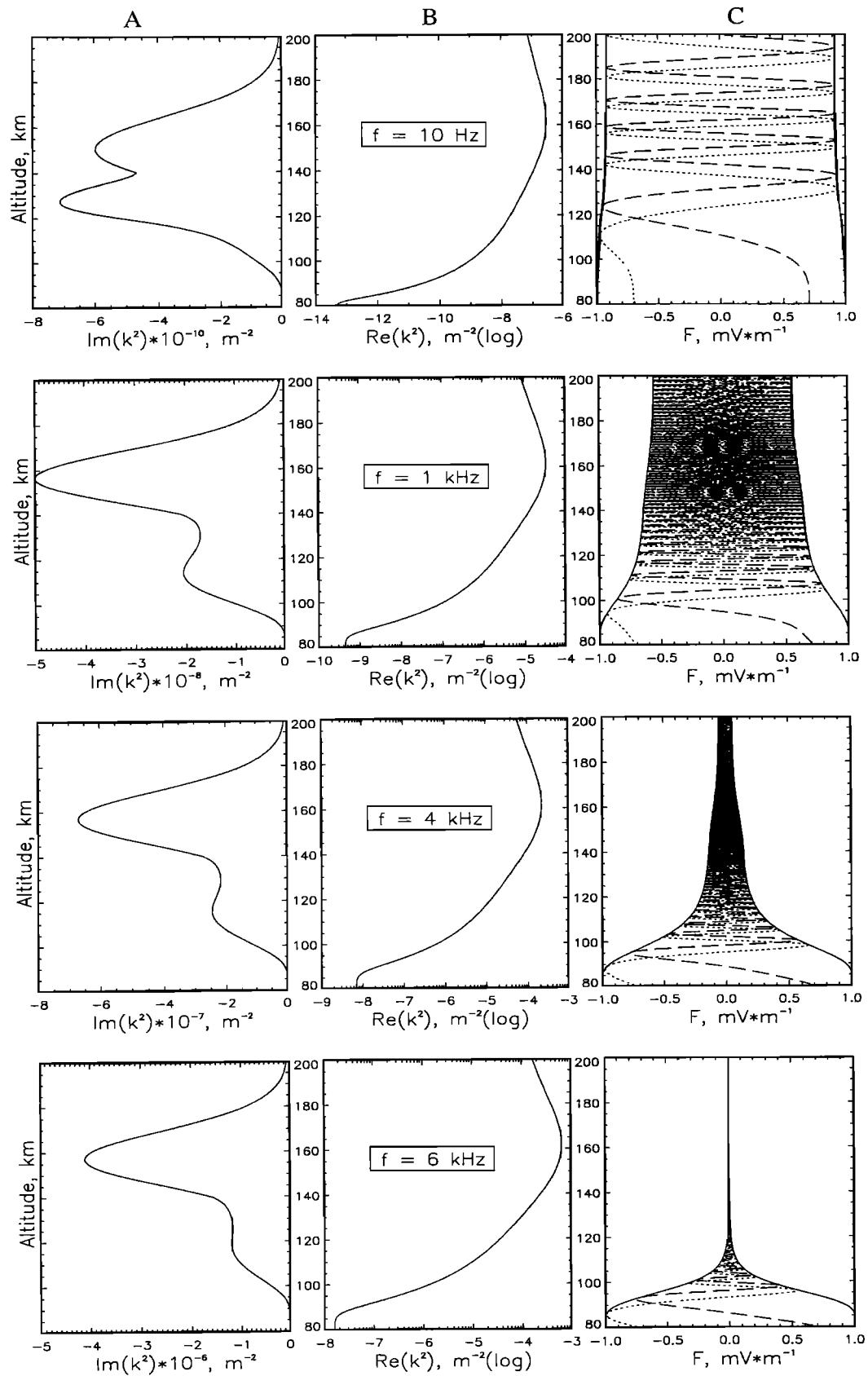


Figure 7. Wave number and wave amplitudes as function of altitude for different frequencies, for the nightside case with a strong magnetic field, and a low solar activity. (a) The imaginary part of the square of the wave number amplitude. (b) The real part of the square of the wave number amplitude. (c) The wave amplitude (the dashed, dotted and solid lines represent the real part, the imaginary part, and the modulus of F , respectively).

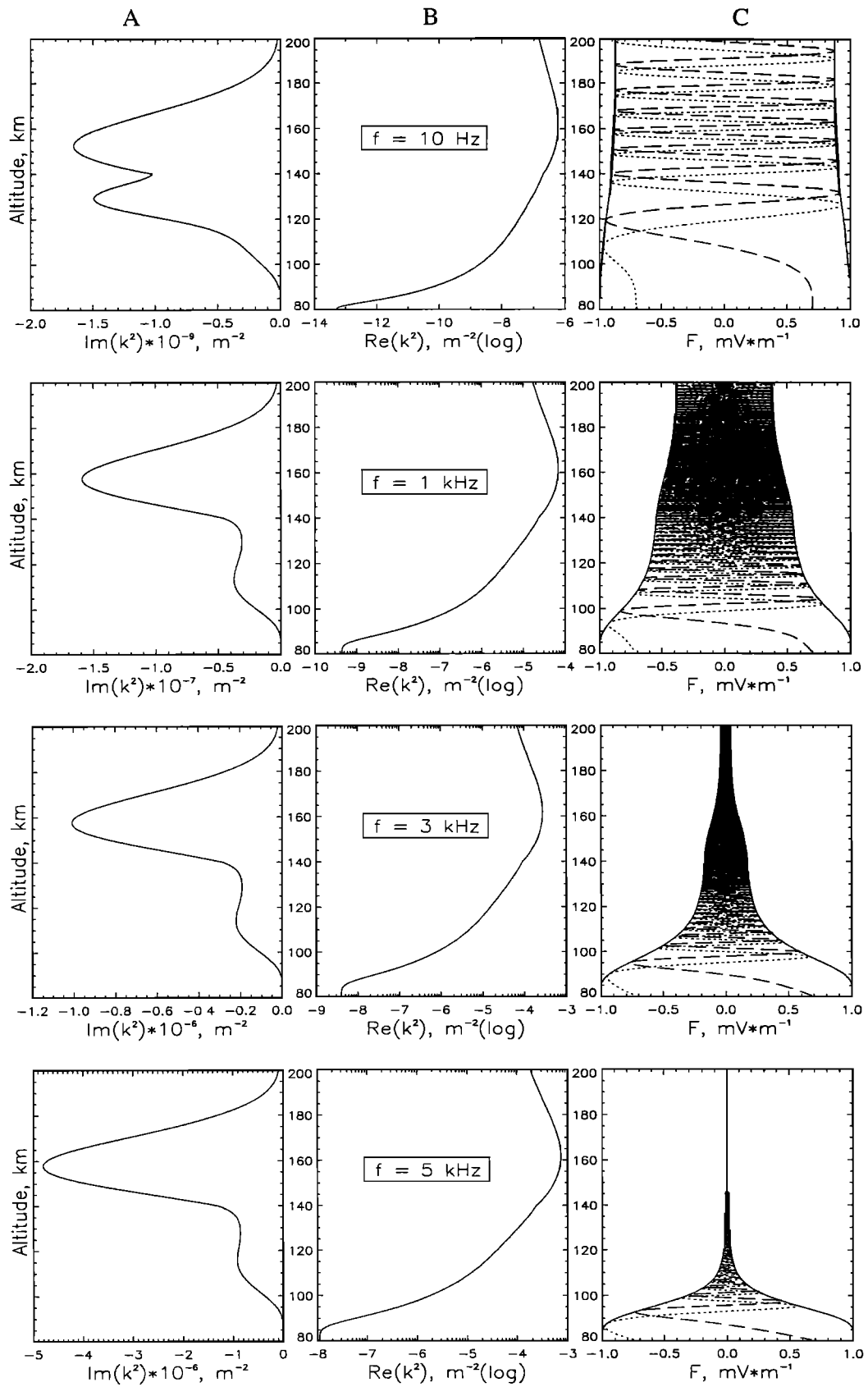


Figure 8. Same as Figure 7, but for high solar activity.

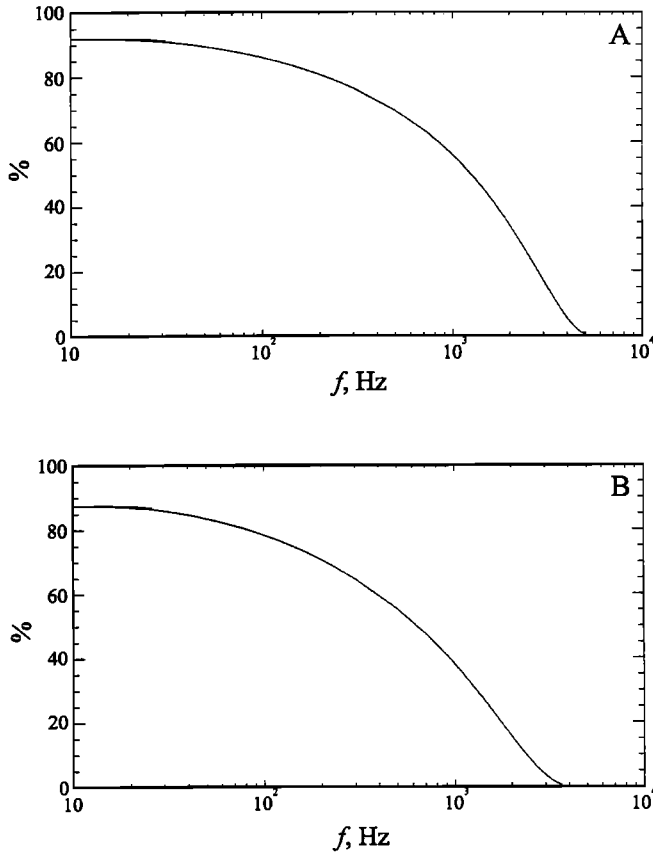


Figure 9. Percentage of the wave amplitude transmitted from 80 to 200 km as function of frequency during (a) low solar activity and (b) high solar activity.

where \mathbf{j} is the current induced by \mathbf{E} . The conductivity tensor σ is

$$\sigma = \begin{vmatrix} \sigma_p & \sigma_H & 0 \\ -\sigma_H & \sigma_p & 0 \\ 0 & 0 & \sigma_0 \end{vmatrix} \quad (\text{A2})$$

where the three parameters, σ_0 , σ_p , and σ_H are called the specific, Pedersen, and Hall conductivities, respectively. The equations of motion for electrons and ions under the action of the Coulomb and Lorentz forces and in the presence of collisions are written [Huba and Rowland, 1993]:

$$\begin{aligned} \frac{\partial \mathbf{v}_e}{\partial t} &= \frac{e}{m_e} [\mathbf{E} + \mathbf{v}_e \times \mathbf{B}_0] - \nu_{en} \mathbf{v}_e - \nu_{ei} (\mathbf{v}_e - \mathbf{v}_i) \\ \frac{\partial \mathbf{v}_i}{\partial t} &= \frac{q_i}{m_i} [\mathbf{E} + \mathbf{v}_i \times \mathbf{B}_0] - \nu_{in} \mathbf{v}_i - \nu_{ie} (\mathbf{v}_i - \mathbf{v}_e) \end{aligned} \quad (\text{A3})$$

where e and m_e are the charge and the mass of electrons, respectively, q_i and m_i are the charge and the mass of ions, respectively, and $\nu_{\alpha\beta}$ is the collision frequency between the species

α and β (e electrons, i ions, and n neutrals). We assume that the temporal variation of the electron velocity \mathbf{v}_e and the ion velocity \mathbf{v}_i is $\propto \exp(i\omega t)$ where ω is the angular frequency. Therefore, using (A3), the equations for the velocity components transverse to the magnetic field are

$$\begin{aligned} v_{ex} &= \frac{E_x}{B_0} \left(\frac{K1}{D} \right) + \frac{E_y}{B_0} \left(\frac{K2}{D} \right) & v_{ey} &= \frac{E_x}{B_0} \left(-\frac{K2}{D} \right) + \frac{E_y}{B_0} \left(\frac{K1}{D} \right) \\ v_{ix} &= \frac{E_x}{B_0} \left(\frac{K3}{D} \right) + \frac{E_y}{B_0} \left(\frac{K4}{D} \right) & v_{iy} &= \frac{E_x}{B_0} \left(-\frac{K4}{D} \right) + \frac{E_y}{B_0} \left(\frac{K3}{D} \right) \end{aligned} \quad (\text{A4})$$

where $D = (\Omega_e^2 + \Lambda_e^2)(\Omega_i^2 + \Lambda_i^2) + (\Lambda_e \Lambda_i - \nu_{ei} \nu_{ie})^2 + 2\Omega_e \Omega_i \nu_{ei} \nu_{ie}$; $K1 = (\Omega_e \Lambda_i + \Omega_i \nu_{ei})(\Lambda_e \Lambda_i - \nu_{ei} \nu_{ie}) + \Omega_e \Omega_i^2 (\Lambda_e - \nu_{ei})$; $K2 = \Omega_e^2 (\Lambda_i^2 + \Omega_i^2) + \Omega_e \Omega_i \nu_{ei} (\Lambda_i + \nu_{ie}) + \Omega_i^2 \Lambda_e \nu_{ei}$; $K3 = (\Omega_e \Lambda_e + \Omega_e \nu_{ie})(\Lambda_e \Lambda_i - \nu_{ei} \nu_{ie}) + \Omega_e^2 \Omega_i (\Lambda_i - \nu_{ie})$; $K4 = \Omega_e^2 (\Lambda_e^2 + \Omega_e^2) + \Omega_e \Omega_i \nu_{ie} (\Lambda_e + \nu_{ei}) + \Omega_e^2 \Lambda_i \nu_{ie}$; $\Lambda_e = \nu_{en} + \nu_{ei} + i\omega$ and $\Lambda_i = \nu_{in} + \nu_{ie} + i\omega$. The usual electron and ion gyrofrequencies are respectively given by $|e|B_0/m_e$ and $\Omega_i = q_i B_0/m_i$, but it must be noted that in all equations and in the calculation of the conductivities, $\Omega_e = eB_0/m_e$ and must be considered as a negative quantity. Using (A1), the components of the current can be written on the following form:

$$\begin{aligned} j_x &= \sigma_p E_x + \sigma_H E_y = n_e e (v_{ex} - v_{ix}) \\ j_y &= \sigma_p E_y - \sigma_H E_x = n_e e (v_{ey} - v_{iy}) \end{aligned} \quad (\text{A5})$$

where n_e is the electron density. Then, combining (A5) with (A4), one obtains the Pedersen and the Hall conductivities:

$$\begin{aligned} \sigma_p &= \frac{n_e e}{B} \frac{(\Lambda_e \Lambda_i - \Omega_e \Omega_i - \nu_{ei} \nu_{ie})(\Omega_i (\nu_{ei} - \Lambda_e) - \Omega_e (\nu_{ie} - \Lambda_i))}{(\Omega_e^2 + \Lambda_e^2)(\Omega_i^2 + \Lambda_i^2) + (\Lambda_e \Lambda_i - \nu_{ei} \nu_{ie})^2 + 2\Omega_e \Omega_i \nu_{ei} \nu_{ie}} \\ \sigma_H &= \frac{n_e e}{B} \frac{\Omega_e^2 \Lambda_i^2 - \Omega_i^2 \Lambda_e^2 - (\Omega_e \nu_{ie} - \Omega_i \nu_{ei})(\Omega_e \Lambda_i + \Omega_i \Lambda_e)}{(\Omega_e^2 + \Lambda_e^2)(\Omega_i^2 + \Lambda_i^2) + (\Lambda_e \Lambda_i - \nu_{ei} \nu_{ie})^2 + 2\Omega_e \Omega_i \nu_{ei} \nu_{ie}} \end{aligned} \quad (\text{A6})$$

The collision frequencies $\nu_{\alpha\beta}$ are given by the usual formulae [Rishbeth and Garriott, 1969; Ratcliffe, 1972; Kelley, 1989]:

$$\begin{aligned} \nu_{en} &= 2.12 \cdot 10^{-16} n_n T_e^{1/2} s^{-1} \\ \nu_{in} &= 2.6 \cdot 10^{-15} n_n M^{1/2} s^{-1} \\ \nu_{ei} &= 3.62 \cdot 10^{-6} n_i T_e^{-3/2} \ln(\Lambda) s^{-1} \\ \nu_{ie} &= \nu_{ei} \frac{m_e}{m_i} \end{aligned} \quad (\text{A7})$$

where $\Lambda = 1.23 \cdot 10^7 T_e^{3/2} n_e^{-1/2}$, n_n is the neutral density, n_i is the ion density, T_e is the electron temperature in K, and M is the mean molecular weight of the ions.

Appendix B: Calculation of the Wave Field

Appendix B presents the solution of equation (4) for the right mode. The first derivative of the F function ($F \propto \exp i(\omega t - kz)$) along the z axis is

$$\frac{\partial F_j}{\partial z} = \frac{F_{j+1} - F_{j-1}}{2\Delta z} = -ik_j F_j \quad (\text{B1})$$

where j is the step index. Then we have the relation:

$$-F_j + 2ik_{j+1}\Delta z F_{j+1} + F_{j+2} = 0, \quad j = 0, 1, \dots, n-2 \quad (\text{B2})$$

If we suppose that a wave with an amplitude A is emitted at the lowest frontier of our system ($z = 80$ km), the above equation for $j = 0$ can be written as

$$2ik_1\Delta z F_1 + F_2 = A \quad (\text{B3})$$

The condition at the highest level supposes an outgoing wave when $z > 200$ km, and using the second derivative of F gives

$$\frac{\partial^2 F_j}{\partial z^2} = \frac{F_{j+1} - 2F_j + F_{j-1}}{\Delta z^2} = -k_j^2 F_j \quad (\text{B4})$$

from which we have, for $j = n$:

$$F_{n-1} + (k_n^2 \Delta z^2 - 2)F_n + F_{n+1} = 0 \quad (\text{B5})$$

The WKB solution for F can be expressed as [Yeh and Liu, 1972; Stix, 1992]

$$F(z) = k(z)^{-1/2} \exp(-i \int_0^z k(z) dz) \quad (\text{B6})$$

If we take the ratio F_{n+1}/F_n , we find that:

$$F_{n+1} = \sqrt{\frac{k_n}{k_{n+1}}} \exp(-i\Delta z \frac{k_n + k_{n+1}}{2}) F_n \quad (\text{B7})$$

Then using (B5), the last equation of our system which gives the relation between F_{n-1} and F_n is

$$F_{n-1} + [k_n^2 \Delta z^2 - 2 + \sqrt{\frac{k_n}{k_{n+1}}} \exp(-i\Delta z \frac{k_n + k_{n+1}}{2})] F_n = 0 \quad (\text{B8})$$

With (B2), (B3), and (B8), we have the following tridiagonal matrix equation to obtain the unknown $F_1, F_2, F_3, \dots, F_n$:

$$\begin{pmatrix} d_1 & 1 & 0 & 0 & \dots & 0 \\ -1 & d_2 & 1 & 0 & \dots & 0 \\ 0 & -1 & d_3 & 1 & \dots & 0 \\ 0 & 0 & -1 & d_4 & \dots & 0 \\ \dots & \dots & \dots & \dots & \dots & \dots \\ 0 & 0 & 0 & \dots & 1 & d_n \end{pmatrix} \times \begin{pmatrix} F_1 \\ F_2 \\ F_3 \\ F_4 \\ \dots \\ F_n \end{pmatrix} = \begin{pmatrix} A \\ 0 \\ 0 \\ 0 \\ \dots \\ 0 \end{pmatrix} \quad (\text{B9})$$

where the complex coefficients d_j are given by

$$d_j = 2ik_j \Delta z \quad \text{for } j = 1, \dots, n-1$$

$$d_n = k_n^2 \Delta z^2 - 2 + \sqrt{\frac{k_n}{k_{n+1}}} \exp(-i\Delta z \frac{k_n + k_{n+1}}{2})$$

To solve (B9) between 80 and 200 km, we have chosen $\Delta z = 50$ m and then $N = 2401$.

The WKB approximation is valid if the variations of the plasma parameters (and then the variation of k) on a distance equal to the wavelength are small. This can be expressed by the following inequality [Swanson, 1989]:

$$\left| \frac{1}{k^2} \left| \frac{dk}{dz} \right| \right| \ll 1 \quad (\text{B10})$$

Acknowledgment. Michel Blanc thanks both referees for their assistance in evaluating this paper.

References

- Acuña, M.H., et al., Magnetic field and plasma observations at Mars: Initial results of the Mars Global Surveyor mission, *Science*, 279, 1676-1680, 1998.
- ELISMA Experimenters, The wave complex on the MARS96 orbiter: ELISMA, *Planet. Space Sci.*, 46, 701-713, 1998.
- Fox, J.L., J.F. Brannon, and H.S. Porter, Upper limits to the nightside ionosphere of Mars, *Geophys. Res. Lett.*, 20, 1391-1394, 1993.
- Fox, J.L., P. Zhou, and S.W. Bougher, The Martian thermosphere/ionosphere at high and low solar activities, *Adv. Space Res.*, 17, (11)203-(11)218, 1996.
- Fry, C.D., and R.J. Yowell, HF radio on Mars, *Communications Quarterly*, 4(2), 13-23, 1994.
- Haider, S.A., Chemistry of the nightside ionosphere of Mars, *J. Geophys. Res.*, 102, 407-416, 1997.
- Huba, J.D., and H.L. Rowland, Propagation of electromagnetic waves parallel to the magnetic field in the nightside Venus ionosphere, *J. Geophys. Res.*, 98, 5291-5300, 1993.
- Kelley, M.C., *The Earth's Ionosphere*, Academic, San Diego, Calif., 1989.
- Melnik, O., and M. Parrot, Electrostatic discharge in Martian dust storms, *J. Geophys. Res.*, 103, 29,109-29,117, 1998.
- Ratcliffe, J.A., *An Introduction to the Ionosphere and Magnetosphere*, Cambridge Univ. Press, New York, 1972.
- Rishbeth, H., and O.K. Garriott, *Introduction to Ionospheric Physics*, Academic, San Diego, Calif., 1969.

- Shinagawa, H., and T.E. Cravens, A one-dimensional multispecies magnetohydrodynamic model of the dayside ionosphere of Mars, *J. Geophys. Res.*, *94*, 6506-6516, 1989.
- Stix, T.H., *Waves in Plasmas*, Am. Inst. of Phys., New York, 1992.
- Swanson, D.G., *Plasma Waves*, Academic, San Diego, Calif., 1989.
- Tsuruda, K., I. Nakatani, and T. Yamamoto, Planet-B mission to MARS-1998, *Adv. Space Res.*, *17*, (12)21-(12)29, 1996.
- Winchester, C., and D. Rees, Numerical models of the Martian coupled thermosphere and ionosphere, *Adv. Space Res.*, *15*, (4)51-(4)68, 1995.
- Yeh, K.C., and C.H. Liu, *Theory of Ionospheric Waves*, *International Geophysics Ser.*, Academic, San Diego, Calif., 1972.

O. Melnik and M. Parrot, Laboratoire de Physique et Chimie de l'Environnement, CNRS, 3A, Avenue de la Recherche Scientifique, 45071 Orléans cedex 02, France. (mparrot@cnr-orleans.fr)

(Received April 23, 1998; revised January 8, 1999; accepted February 5, 1999.)